You may also be interested in:

XXIII AIVELA Annual Meeting 2015

IOP Publishing

IOP Conf. Series: Journal of Physics: Conf. Series **778** (2017) 012005

doi:10.1088/1742-6596/778/1/012005

# Water Spray Flow Characteristics Under Synthetic Jet Driven By a Piezoelectric Actuator

**L. Marchitto[1], G. Valentino[1], M. Chiatto[2], L. de Luca[2]**

[1] Istituto Motori, CNR - NAPOLI – ITALY,

[2] Dept. of Industrial Engineering, University of Naples "Federico II" - NAPOLI - ITALY

E-mail: l.marchitto@im.cnr.it

**Abstract**. Particle Image Velocimetry (PIV) and Phase Doppler Anemometry (PDA) have been applied to investigate the droplets size and velocity distribution of a water spray, under the control of a piezo-element driven synthetic jet (SJ).

Tests were carried out under atmospheric conditions within a chamber test rig equipped with optical accesses at two injection pressures, namely 5 and 10 MPa, exploring the variation of the main spray parameters caused by the synthetic jet perturbations.

The SJ orifice has been placed at 45° with respect to the water spray axis; the nozzle body has been moved on its own axis and three different nozzle quotes were tested. PIV measurements have been averaged on 300 trials whereas about $10^5$ samples have been acquired for the PDA tests. For each operative condition, the influence region of the SJ device on the spray has been computed through a T-Test algorithm.

The synthetic jet locally interacts with the spray, energizing the region downstream the impact. The effect of the actuator decreases at higher injection pressures and moving the impact region upwards. Droplets coalescence can be detected along the synthetic jet axis, while no significant variations are observed along a direction orthogonal to it.

## 1. Introduction

Spray-based technology has been undergoing continuous evolution in the last decades, covering a wide spread of applications such as internal combustion engines, turbines, fire control systems, as well as agriculture machines and several manufacturing processes. The technological improvement has been mainly focused on pressure control, size and nozzle-hole number, tip penetration length and cone angle. At the same time, the opportunity of directly managing spray formation and its characteristics has gained much interest among active flow control methods using different types of actuators [1]. A first classification of spray control mechanisms was made by Photos and Longmire [2] depending on the way of interacting with a spray: direct, if a direct impact between the control mechanism and droplets occurs; indirect, if the interaction is produced by controlling the space and the size of fluid structures. Among them, synthetic jet actuators seem to be a promising technology for spray direct control, showing the potential to affect their global behavior as well as their characteristics at local level.

As depicted in Figure 1, a synthetic jet (SJ) is an electromechanical device consisting of a relatively small cavity, which is sealed from one side by an elastic vibrating diaphragm, and from the other one, is linked to the external environment through a slot or an orifice. The diaphragm (membrane, wall) oscillation, generally driven by a piezo-ceramic element, produces periodic cavity volume changes,

with corresponding pressure variations, that cause subsequent alternation of ejection and suction phases of fluid across the orifice, [3,4,5]. During the expulsion phase a vortex ring forms near the orifice exit which, under favorable operating conditions [6], convects downstream by its self-induced velocity towards the far field. Few cycles are required for the formation of a train of vortex rings that interact with each other and break up due to the viscous dissipation eventually "synthesizing" a turbulent jet always directed downstream, [7]. A major characteristic of this jet lies in a zero-net mass-flux during an operating cycle, but in a non-zero momentum flux. Furthermore, it does not require any continuous supply of fluid for its generation, because it is synthesized directly from the surrounding fluid.
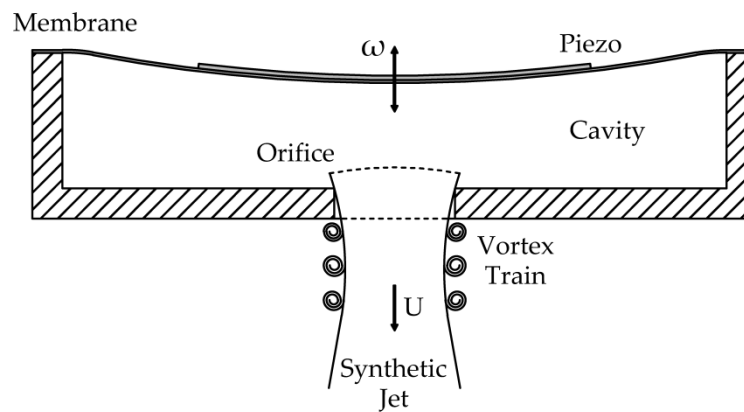


**Figure 1.** Sketch of the synthetic jet device.

The effect of a SJ actuator on an air atomized spray was investigated by Pavlova et al. [8], quantified through a non-dimensional parameter: the momentum coefficient, defined as:

$$C_\mu = \frac{A_j \overline{U}_j^2}{A_s \overline{U}_{so}^2}$$

(1)

where $A_j$ and $A_s$ are the orifice area of the synthetic jet and the spray, respectively, whereas $\overline{U}_{so}$ is the average air exit velocity at the spray orifice, and $\overline{U}_j$ is the synthetic jet average orifice velocity. The latter is known as:

$$U_j = \frac{L}{T}$$

(2)

in which $T$ is the actuator period and $L$ is the stroke length, defined as the integral of the velocity at the orifice exit (spatially averaged), $U_j$, over the ejection phase of the cycle only:

$$L = \int_0^{T/2} U_j(t) dt$$

(3)

This paper aims to investigate the effect of a synthetic jet actuator on a continuous water spray. The experimental apparatus, the methodologies applied and the characteristics of the actuator will be presented in Section 2. Section 3 will be dedicated to the definition of a new momentum coefficient, which takes into account the densities of the operating fluids, and it is followed by the results in terms of spray velocity and droplets distribution fields. Finally, conclusions will be reported in Section 4.

## 2. Experimental Apparatus and Procedure

The spray behavior has been characterized through optical diagnostic techniques. Considering the low droplets velocity and size, a statistical analysis has been applied to establish the spray regions that have been effectively influenced by the SJ device.

Particle Image Velocimetry (PIV) and Phase Doppler Anemometry (PDA) techniques have allowed to measure spray velocity and droplets mean diameter, respectively. Figure 2 shows the PIV experimental apparatus and the water injection system. The latter is composed of a high pressure pump used to supply water to a one-hole misting nozzle (300 μm diameter), which injects the working fluid in a 4500 cm$^3$ quiescent optically accessible tank at ambient temperature and pressure. The injector works in continuous mode and its working regime is managed by a rubber ball connected to a spring; when the liquid pressure exceeds the elastic spring force, the ball moves allowing the liquid passage. For this reason the spray can be considered continuous and stationary.
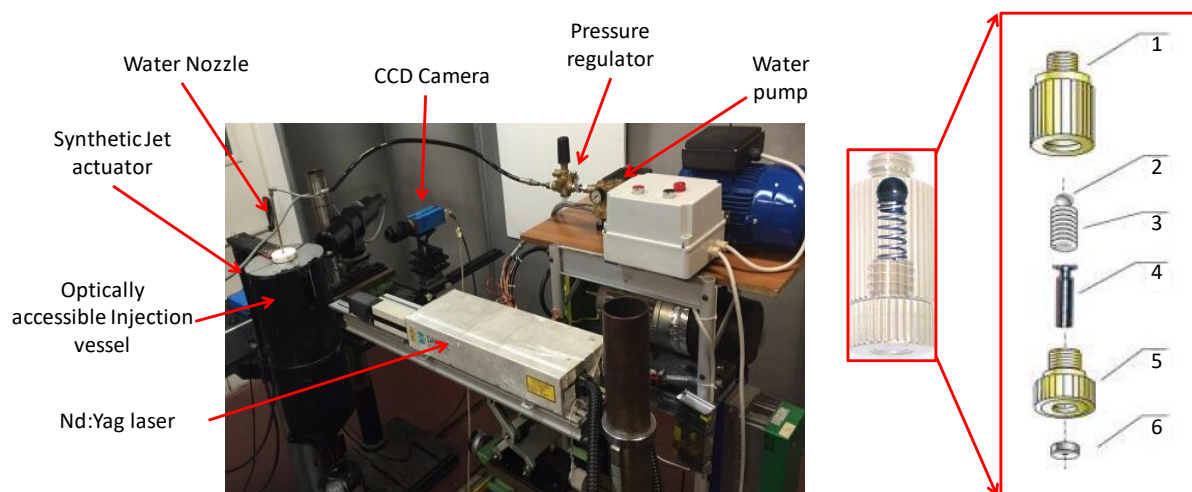


**Figure 2.** PIV and injection system experimental apparatus (left) - Hole misting nozzle sketch (right).

A twin head pulsed Nd:YAG laser (532 nm wavelength), has been synchronized with a CCD camera in order to perform PIV measurements. An appropriate optical path converts the laser beam in a sheet (0.2 mm of thickness and 60 mm of height) crossing the spray axis, coincident with the vessel one. The light scattered by the spray has been collected by the CCD camera, mounted perpendicularly to it. Images (2048 x 2048 pixel of resolution and 7.4 x 7.4 μm of pixel size) have been acquired in double frame mode in order to record a pair of them for each trigger signal, with a frequency of 1 Hz, for a total of 300 couples of images. An adaptive correlation process has been applied to track the droplets clusters and to estimate their speed. This method uses an initial interrogation area (IA) having a size N times the final IA. Each intermediary result is used as information for the next IA of smaller size, until the smallest IA size is reached. A 32×32 pixels final IA has been reached starting by a size of 128×128 pixels. A local validation procedure has been applied in order to minimize false sample vectors and a 50 % overlap of interrogation areas has been set to recover the loss of vector field resolution. Furthermore, the analysis has been completed by the Peak Height Validation criterion and the Local Neighborhood Validation method.

PDA tests, whose apparatus is shown in Fig. 3, have been performed in the same tank used for PIV experiments. The set-up consists in an argon-ion laser, with operative wavelengths of 514.5 and 488 nm, a transmitting probe with a focal length of 310 mm, beam separation of 65 mm, and receiving optics placed with an angle of 30° with respect to the axis of the transmitting probe in order to maximize the signal-to-noise ratio.
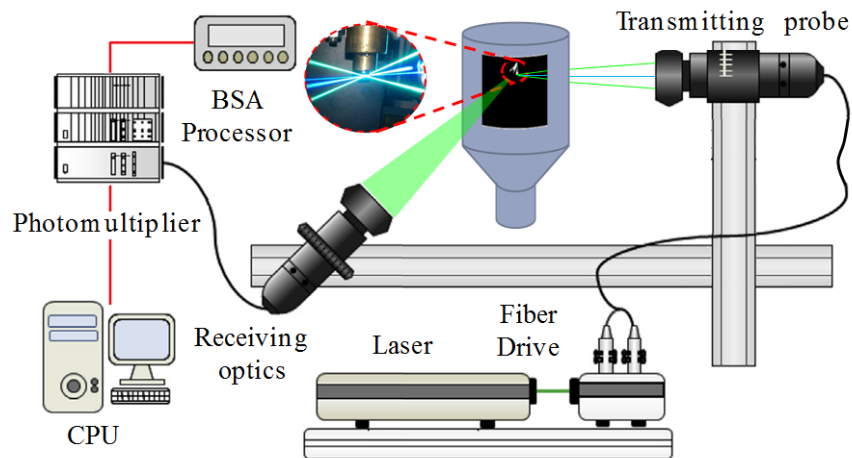
XXIII AIVELA Annual Meeting 2015

IOP Publishing

IOP Conf. Series: Journal of Physics: Conf. Series **778** (2017) 012005

doi:10.1088/1742-6596/778/1/012005

**Figure 3.** PDA experimental apparatus.

The probes have been mounted on a tridimensional translation slide, allowing the acquisition at different locations inside the spray with micrometric accuracy. An acquisition time of 300 s and a number of samples equal to 100000 were required to collect an adequate data sample for statistical analysis. All the experiments have been conducted in the atmospheric chamber test rig with a drain at the bottom driven by a vacuum pump to remove the moisture. Further details about PIV and PDA equipment can be found in [9].Tests have been carried out under quiescent conditions at two injection pressures, namely 5 and 10 MPa, exploring the effect produced by the synthetic jet perturbations on the droplets velocity and size. The inclination of the synthetic jet axis has been equal to 45° with respect to the nozzle axis direction, as shown in Figure 4. The relative quote of synthetic jet with respect to the water nozzle has been varied from a maximum ($\Delta h = 0$ mm) corresponding to 11.6 mm distance between the nozzle and actuator orifices up to 1.6 mm ($\Delta h = 10$ mm) with a step of 5 mm.
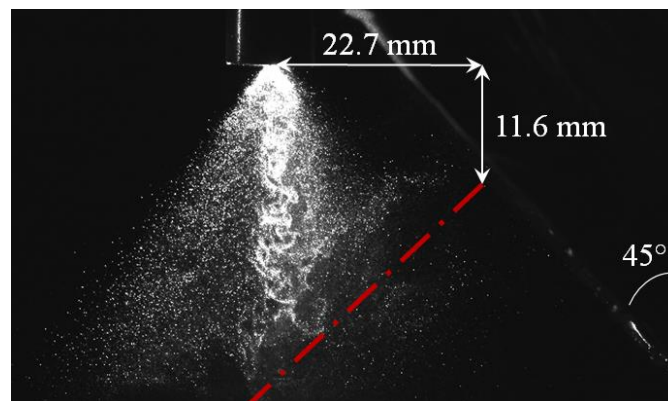


**Figure 4.** Relative position between the nozzle and the synthetic jet actuator, ($\Delta h=0$).

PIV Measurements have been carried out at all set positions, for a total of 12 tests (summarized in Table 1), whereas PDA tests at the intermediate one. More in detail, since PDA allows only punctual measurements, two axis, one coincident with that of the synthetic jet actuator and one perpendicular to it, have been chosen to acquire values.

**Table 1.** PIV operative conditions.

|        | Injection Pressure, $P_i$ | Nozzle Height, $\Delta h$ |
|--------|---------------------------|---------------------------|
| Case 1 | 5 MPa                     | 0 mm                      |
| Case 2 | 10 MPa                    | 0 mm                      |
| Case 3 | 5 MPa                     | 5 mm                      |
| Case 4 | 10 MPa                    | 5 mm                      |
| Case 5 | 5 MPa                     | 10 mm                     |
| Case 6 | 10 MPa                    | 10 mm                     |

The actuator design is based on the work of de Luca et al. [**Errore. Il segnalibro non è definito.**], whose characteristics are reported in Table 2. It is a modular structure device (Figure 5), allowing independent variations of cavity diameter and height, orifice diameter, and piezo-electric diaphragm. Its features and actuation frequency (f=2404 Hz for all experimental tests) have been chosen to maximize the exit jet velocity, and so the momentum coefficient, which is the main parameter for spray interaction.

**Table 2.** Synthetic jet actuator characteristics.

| | |
|---------------------------|----------|
| Cavity Diameter, $D$      | 35 mm    |
| Cavity Height, $H$        | 3 mm     |
| Orifice length, $l$       | 2 mm     |
| Orifice length, $d$       | 2 mm     |
| Supply Voltage, $V$       | 70 V     |
| Actuation frequency, $f$  | 2404 Hz  |
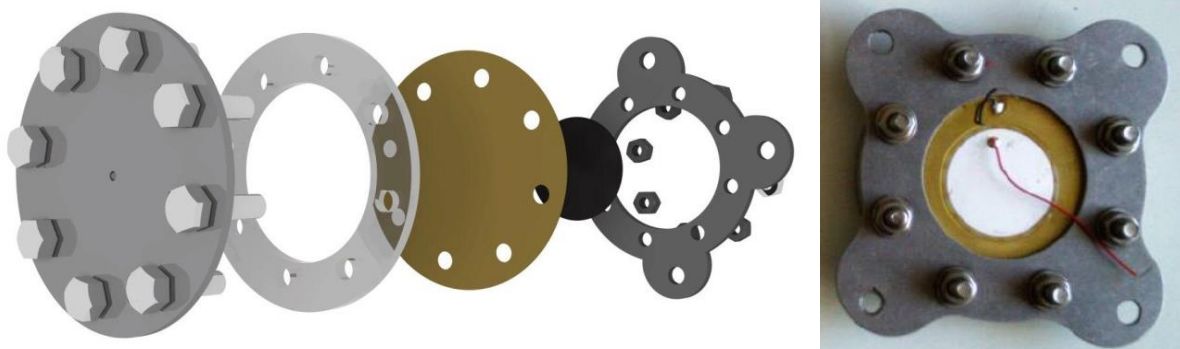


**Figure 5.** brass synthetic jet actuator (left) - exploded 3D view (right).

Considering the low speed range of water sprays and the statistic nature of PIV measurements, a T-test, implemented in *MATLAB*, has been performed to discriminate between the stochastic spray variability and the perturbation produced by the synthetic jet [10]. For each operative condition two

vector maps, corresponding to active synthetic jet and free water spray cases, have been estimated as the average on 300 trials. A point-by-point comparison of the maps has been performed through the T-test code on the single interrogation areas.

The T-test is based on the assumptions that each sample population $X_i$ follows a normal distribution with mean value $\mu$ and variance $\sigma^2$ and the two sample populations should have the same variance.

First, a Normal Probability Plot has been built in order to estimate if each set of experimental data follows a normal distribution. The experimental data were sorted in ascending order and for each sorted value the Cumulative Distribution Function (CDF) was evaluated through the following estimator:

$$\hat{F}(x_i) = \frac{i}{n+1} \tag{4}$$

Where $x_i$ is the *i-th* sorted value of sample *X* and *n* is the sample dimension. The Cartesian product $(x_i, \hat{F}(x_i))$ has been compared to the linearized analytical CDF distribution. The method of ordinary least squares has been used to approximate the experimental distribution to the analytical one. All the distributions whose correlation coefficient between the experimental values and the least squares line is over than 0.90 have been considered normal. Once the normal distribution of samples has been confirmed, a F-test has been performed for verifying the assumption that the two sample populations have the same variance. The well-known Fisher-Snedecor distribution relation has been used as test statistic:

$$\frac{S_1^2}{S_2^2} \frac{\sigma_2^2}{\sigma_1^2} = Z_{n-1,m-1} \tag{5}$$

where $S_1^2$ and $S_2^2$ represent the unbiased sample variance of the aleatory variables $X_1$ and $X_2$ respectively, *n* and *m* are the sample dimensions. The unbiased sample variance can be written as:

$$S^2 = \frac{\sum_{i=1}^{n}(X_{1i} - \bar{X}_1)^2 + \sum_{i=1}^{m}(X_{2i} - \bar{X}_2)^2}{n+m-2} \tag{6}$$

where $X_{1i}$ and $X_{2i}$ are respectively the i-th aleatory variables of the sampling of the sample populations $X_1$ and $X_2$ which determinate the mean sample aleatory variables $\bar{X}_1$ and $\bar{X}_2$.

The null hypothesis of equality of variances is considered true if the actual value is below 0.05. Once all the assumptions are verified the T-test can be performed through the T-distribution, used as test statistic:

$$\frac{(\bar{X}_1 - \bar{X}_2) - (\mu_1 - \mu_2)}{S\sqrt{\frac{1}{n} + \frac{1}{m}}} = T_{n+m-2} \tag{7}$$

The same threshold as for the F-test has been set for the null hypothesis of equality of means. Hence, if the null hypothesis is not satisfied the means difference can be attributed to the synthetic jet effect. Repeating this analysis for a large number of points in the spray domain, it has been possible to distinguish the region in which the synthetic jet is effective from another where the effect is not relevant, (Figure 6).
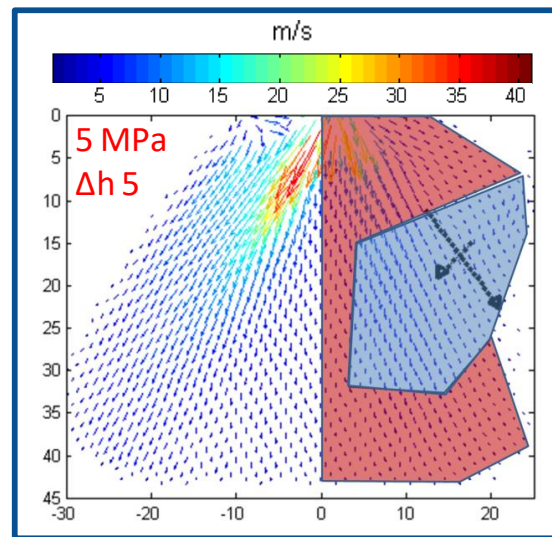
**Figure 6.** Influence region (blue) of synthetic jet actuator on the averaged velocity vector field at 5 MPa injection pressure, Δh 5 mm.

## 3. Results and Discussion

### 3.1. Results and Discussion

The synthetic jet actuator has been designed in order to work in direct mode. For this reason it is important that the air moved by the actuator is strong enough to modify the particles trajectory by means of a direct impact with them. The momentum coefficient $C_\mu$, defined in eq. (1), is the ratio of the synthetic jet momentum to the spray momentum due to the air part only.

In this paper a generalization of this definition is introduced in order to take into account the differences in density between water, used for spray, and air, working fluid of the SJ device. The re-defined momentum coefficient $C_\mu^*$ results to be:

$$C_\mu^* = \frac{\dot{m}_j \overline{U}_j}{(\dot{m}_a + \dot{m}_l)\overline{U}_{so}} \tag{8}$$

Where $\dot{m}_j$ is the synthetic jet mass flow rate, $\dot{m}_a$ is the mass flow rate of the air spray component and $\dot{m}_l$ is the mass flow rate of the liquid spray component. Note that if the spray is almost completely composed by air, such as in an air atomized one, the expression can be simplified, recovering the eq. (1). For the present activity $C_\mu^*$ have been estimated equal to 4.46 for an injection pressure of 5 MPa and 2.07 for 10 MPa case.

### 3.2. Spray velocity field

PIV measurements results are reported in Figs. 7-18. In particular, odd figures contain spray velocity fields: the first picture represents the statistical analysis result, whereas the others show a comparison between the zoomed right side of the domain, without and with actuation. The blue region is the influence area of the actuator on the velocity magnitude, while the red one represents the part in which the jet effect is negligible. The arrows, instead, represent the directions along which the velocity profiles have been extracted: the first one coincident with the synthetic jet longitudinal axis, the latter perpendicular to the former. These results are plotted in the even figures.

The jet produced by the device is clearly visible in zoomed pictures due to the presence of water droplets in the injection chamber which, detached from the spray, have been dragged by the air motion

and can be considered as tracers. It is interesting to notice a difference in the magnitude of the synthetic jet velocity between the 5 MPa and 10 MPa cases; this can be explained considering the higher atomization rate and the greater amount of water particles at 10 MPa near the synthetic jet orifice caused by the increased flow rate. This results in a higher amount of droplets in the region immediately out of the synthetic jet orifice, where the air speed is generally higher, improving measurements accuracy.

When injection pressure rises up (Figs. 7 and 9), it is possible to note an overall increase in velocity magnitude for both cases, with and without actuation. More in detail, considering the velocity fields, the region of influence (blue one) becomes smaller, according with the two calculated $C_\mu^*$ coefficients. As expected at 10 MPa the droplets have higher momentum flux than the case at 5 MPa and so altering their motion becomes more difficult. On the other hand, analysing the velocity profiles, at 5 MPa (Fig. 8) the actuator produces a constant droplets speed increase of about 2 m/s along the longitudinal axis.

At 10 MPa (Fig. 10), instead, the velocity enhancement lowers toward the water spray core, confirming the reduction of the influence. Looking at the transversal axis, for both investigated pressures a significant speed gain has been found. This outcome is characterized by a local maximum located on the synthetic jet axis, while the speed difference between the controlled and uncontrolled cases is almost negligible at about 5 mm distance from the center (borderline of the no-influence region).

The velocity vector fields at 5 and 10 MPa for Δh=5 mm are reported in Figures 11 and 14. Moving downward the injector, the air flow impacts against the spray in a region closer to the nozzle. As expected, the higher water momentum flux induces a reduction of the air flow-water spray interaction, both in terms of interaction region area and of velocity difference. Furthermore, note that at 5 MPa injection pressure the effect of the synthetic jet along its longitudinal axis resulted in a droplet speed increase of about 1 m/s (Figure 12, left).

At 10 MPa injection pressure, such an increase is almost negligible, exhibiting only a slight difference just on the spray edge (between 1 to 2 mm on the spray edge) (Figure 14, left). Looking at the cross axis profiles, as for the Δh=0 mm case, a relatively small velocity increase is detected on the jet axis for injection pressure of 5 MPa (Figure 12, right), while the speed difference is almost negligible at 10 MPa (Figure 14, right).

The difference in the water droplets velocity, between the 5 and 10 MPa configurations, results in a different way in which the jet approaches to the spray. Due to the higher interaction at lower injection pressure, the synthetic jet seems to merge with the spray even upstream the contact point and the result is a slight impact with a totally energization; this allows a global velocity raise and an increase in spray diffusion. On the contrary, at higher injection pressure the impact is sharper because the jet is not able to influence the motion of the droplets, which follow their standard trajectory; this produces a velocity increase limited to the region near the impact point only.

The velocity vector fields at 5 and 10 MPa for Δh=5 mm are reported in Figures 15 and 18. Moving the injector to the lowest position results in a region of air-water impact immediately out of the nozzle hole. On the other hand the distance between synthetic jet orifice and spray is maximum, lowering the air speed in the region of impact. At 5 MPa the air flow-water spray interaction appears to be similar to the case 3, both in terms of interaction region area and of velocity difference. Again, the effect of the synthetic jet along its longitudinal axis resulted in a droplet speed increase of about 1 m/s (Figure 16, left). By increasing the injection pressure, the momentum flux further increases and the effect of the synthetic jet is almost negligible as shown in figure 18. This behavior could be expected considering that the region impact is immediately out of the nozzle hole, where the spray is compact and break up is still occurring. Moreover the higher distance between the synthetic jet actuator and water spray lowers the air velocity in the impact region and consequently its influence.
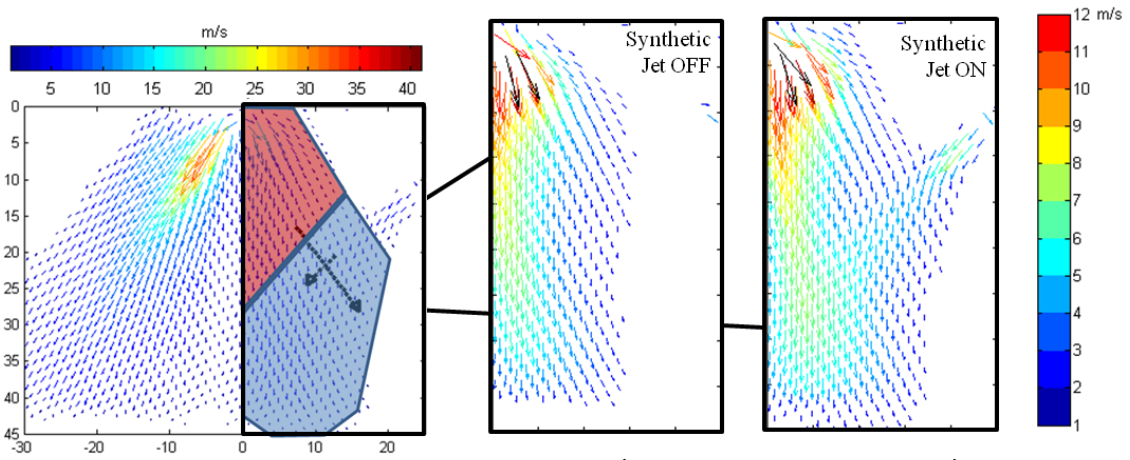
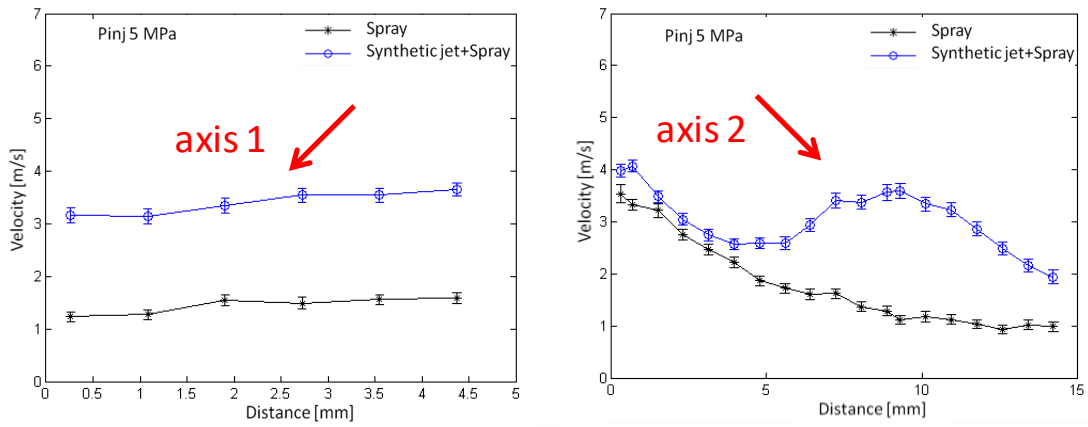**Figure 7.** Case 1: Spray velocity field, $\left(P_{inj} = 5\ MPa, \Delta h = 0\ mm\right)$.



**Figure 8.** Case 1: Profile plots: longitudinal axis (left) – transversal axis (right), $\left(P_{inj} = 5\ MPa, \Delta h = 0\ mm\right)$.
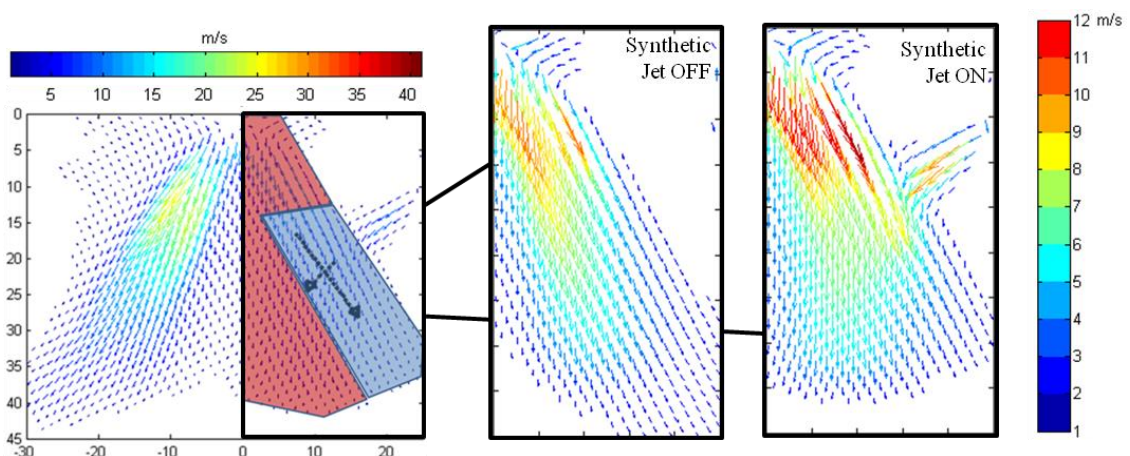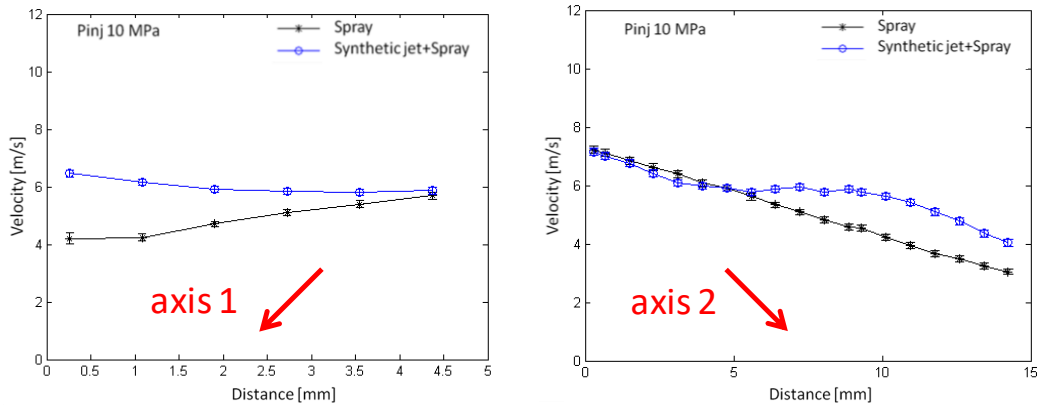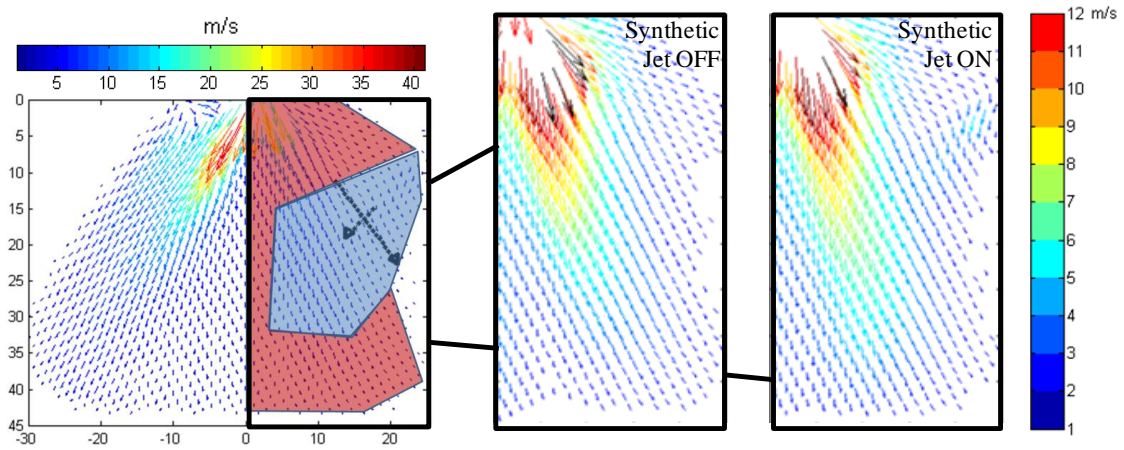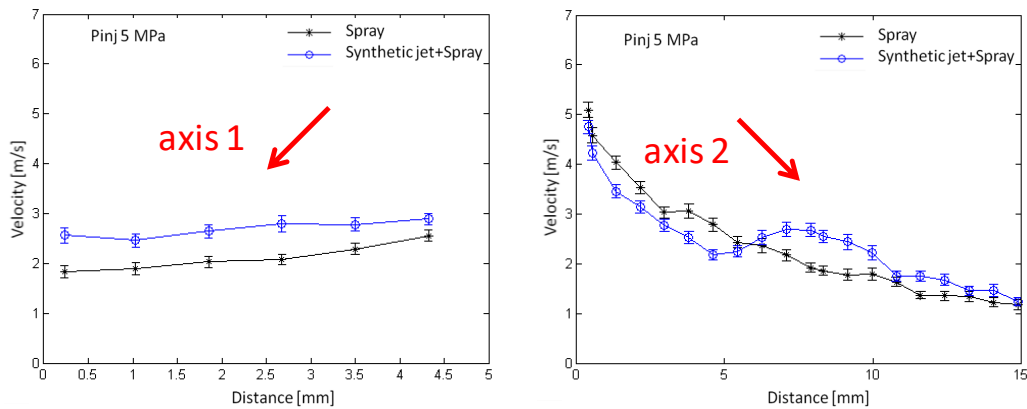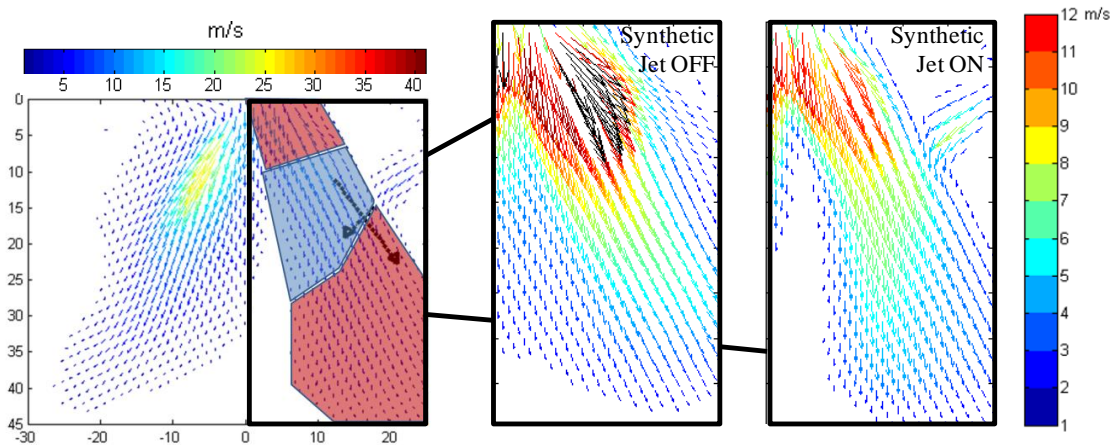


**Figure 9.** Case 2: Spray velocity field, $\left(P_{inj} = 10\ MPa, \Delta h = 0\ mm\right)$.
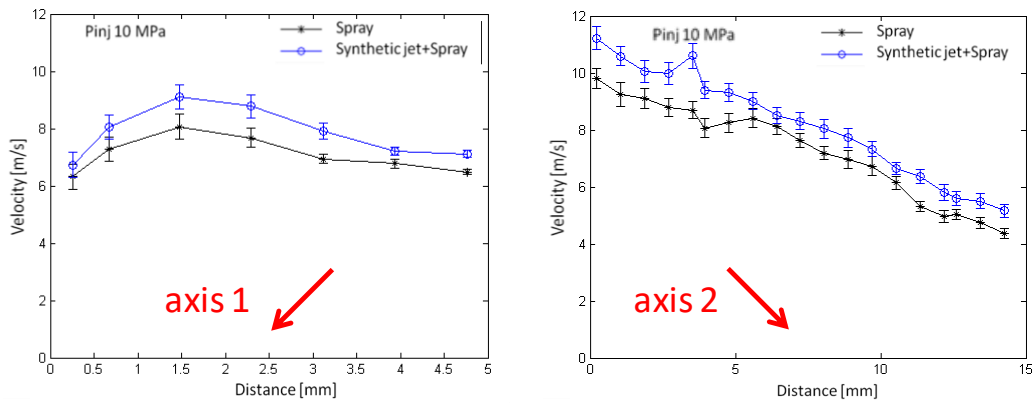
**Figure 10.** Case 2: Profile plots: longitudinal axis (left) – transversal axis (right), $\left(P_{inj} = 10\ MPa, \Delta h = 0\ mm\right)$.



**Figure 11.** Case 3: Spray velocity field, $\left(P_{inj} = 5\ MPa, \Delta h = 5\ mm\right)$.



**Figure 12.** Case 3: Profile plots: longitudinal axis (left) – transversal axis (right), $\left(P_{inj} = 5\ MPa, \Delta h = 5\ mm\right)$.
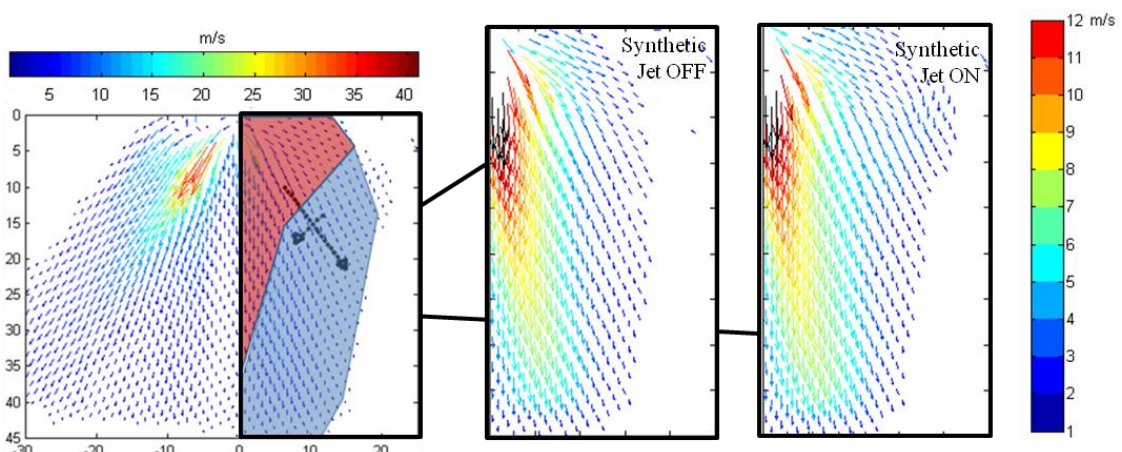
**Figure 13.** Case 4: Spray velocity field, $\left(P_{inj} = 10\ MPa, \Delta h = 5\ mm\right)$.
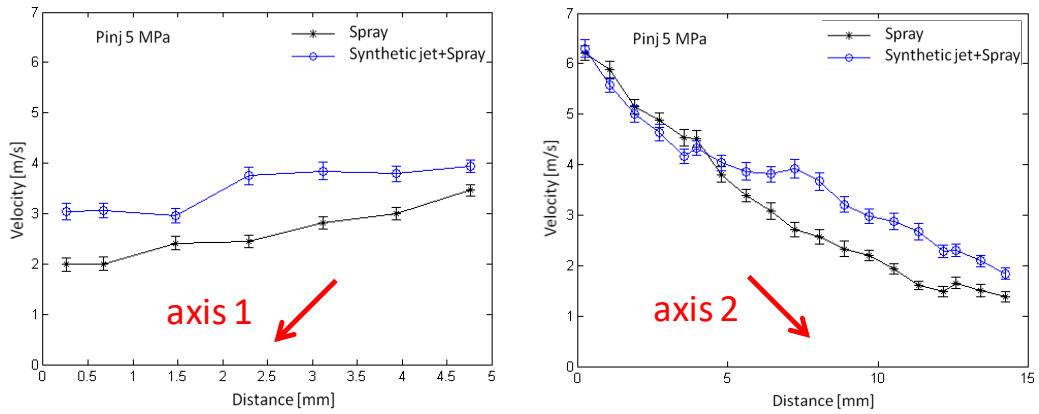


**Figure 14.** Case 4: Profile plots: longitudinal axis (left) – transversal axis (right), $\left(P_{inj} = 10\ MPa, \Delta h = 5\ mm\right)$.



**Figure 15.** Case 5: Spray velocity field, $\left(P_{inj} = 5\ MPa, \Delta h = 10\ mm\right)$.

**Figure 16.** Case 5: Profile plots: longitudinal axis (left) – transversal axis (right), $\left( P_{inj} = 5 \, MPa, \Delta h = 10 \, mm \right)$.
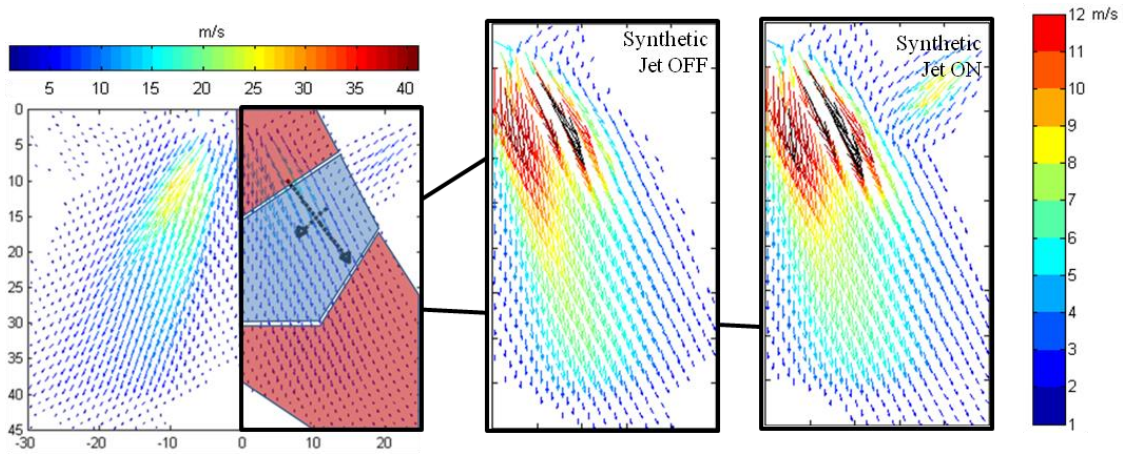


**Figure 17.** Case 6: Spray velocity field , $\left( P_{inj} = 10 \, MPa, \Delta h = 10 \, mm \right)$.



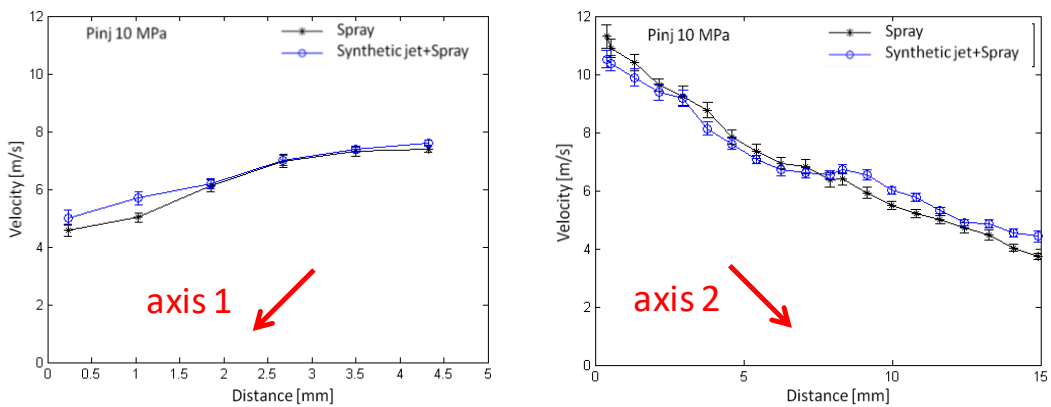**Figure18.** Case 6: Profile plots: longitudinal axis (left) – transversal axis (right), $\left( P_{inj} = 10 \, MPa, \Delta h = 10 \, mm \right)$.

*3.2 Spray droplets distribution*

PDA measurements have been performed to achieve information about the synthetic jet influence on the atomization process. This technique is able to determine the diameter distribution of the particles which cross the measurement volume, obtaining a local estimation. For this reason it is not possible to characterize the whole spray but the choice of critical and significant points is required. Tests have been carried out for the two injection pressures at Δh=5 mm condition. As for PIV measurements, tests have been repeated with and without the actuator. In particular, 4 points have been set along the longitudinal axis, whereas 7 along the transversal one. The resulted profile plots are reported in Figure 19: the left picture is referred to the longitudinal axis whereas the right one to the transversal one.

As expected the higher injection pressure resulted in an enhanced atomization. Along the longitudinal axis the mean diameter lowers from about 40 μm to less than 35 μm; whereas along the transversal axis values range from about 35 μm to 50 μm undergoing a downward jump of about 10 μm. This is related to the growing of the aerodynamic forces at 10 MPa, which enhances the break-up process.

Looking at the effect of the synthetic jet, an increase in droplets diameter is produced along the longitudinal axis for both pressure conditions. It can be related to a coalescence effect: the particles which move away from the spray periphery are pushed back by the synthetic jet towards to spray axis, colliding with the droplets behind. The synthetic jet is not so efficient to transfer to the particles a high momentum exchange, therefore droplets disintegration is limited and coalescence occurs. This result is in accordance with the work of Pavlova et al. [8].

On the contrary, along the transversal axis the influence of the synthetic jet is almost negligible. Whereas at 10 MPa condition the coalescence effect seems to be still present, at 5 MPa the two curves are practically overlapping.
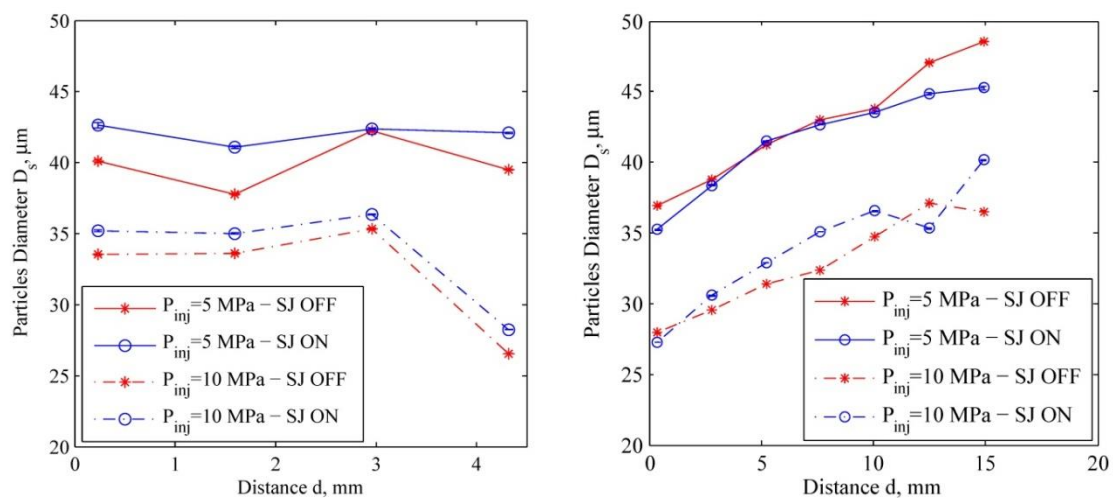


**Figure 19.** Average droplets diameter (D10) profile plots: longitudinal axis (left) – transversal axis (right).

## 4. Conclusions

PIV results show that the synthetic jet interacts with the spray locally, energizing the region downstream of the impact and producing higher velocity droplets. This effect tends to reduce increasing the injection pressure, in agreement with the estimated momentum coefficients, due to a high droplets momentum values, which makes their motion alteration more difficult. Moving downward the injector, the air flow impacts against the spray in a region closer to the nozzle. The higher water momentum flux induces a reduction of the air flow-water spray interaction, both in terms of interaction region size and velocity difference.

PDA measurements exhibits a coalescence effect on the droplets distribution along the actuator axis. The influence is higher at the lowest injection pressure. On the contrary, along a transversal axis significant variations are not revealed. This behaviour has likely to be attributed to the relatively long distance between the jet exit orifice and the water spray region where the breakup process is completely accomplished.

[1]     Cattafesta L N, Sheplak M 2011 Actuators for active flow control *Annual Review of Fluid Mechanics vol.43* pp 247-272.

[2]     Pothos S, Longmire E K 2002 Control of a particle-laden jet using a piezo-electric actuator *11th International Symposium on Applications of Laser Techniques to Fluid Mechanics, Lisbon*.

[3]     de Luca L, Girfoglio M, Coppola G 2014 Modeling and experimental validation of the frequency response of synthetic jet actuators. *AIAA Journal vol 52* n.8 pp 1733-1748.

[4]     Girfoglio M, Greco C S, Chiatto M, de Luca L 2015 Modelling of efficiency of synthetic jet actuators *Sensors and Actuators A: Physical vol 233* pp 512-521.

[5]     de Luca L, Girfoglio M, Chiatto M and Coppola G 2016 Scaling properties of resonant cavities driven by piezo-electric actuators *Sensors and Actuators A: Physical vol 247* pp 465–474.

[6]     Holman R, Utturkar Y, Mittal R, Smith B L, Cattafesta L 2005 Formation criterion for synthetic jets *AIAA journal vol 43* n 10 pp 2110-2116.

[7]     Smith B L, Glezer A 1998 The formation and evolution of synthetic jets *Physics of Fluids (1994-present) vol 10* n.9 pp 2281-2297.

[8]     Pavlova A A, Otani K, Amitay M 2008 Active control of sprays using a single synthetic jet actuator *International journal of heat and fluid flow*, *vol 29* n.1 pp 131-148.

[9]     Marchitto L, Valentino G, Merola S S, Tornatore C 2015 Characterization of alcohol sprays from multi-hole injector for DISI engines through PIV technique (No. 2015-01-0927) SAE Technical Paper.

[10]    Sepe V 2015 Optical Investigation of a Water Spray Controlled by a Synthetic Jet Device *Master's Degree Dissertation* University of Naples "Federico II".